



## Preparation, physicochemical characteristics and bioactivity of citron peel/chitosan nanocomposite by photocatalysis

S. Amutha<sup>1</sup>, E. Amutha<sup>1</sup>, S. Rajadurai<sup>2</sup>, E. Pushpalakshmi<sup>1</sup>, M. Vanaja<sup>1</sup>,  
G. Annadurai<sup>\*1</sup>

<sup>1</sup>*Sri Paramakalyani Centre of Excellence in Environmental Sciences, Manonmaniam Sundaranar University, Alwarkurichi, Tamil Nadu, India*

<sup>2</sup>*Sri Paramakalyani College, Manonmaniam Sundaranar University, Alwarkurichi, Tamil Nadu, India*

Article published on September 09, 2023

**Key words:** Chitosan, Fruit peel nanocomposite, Antibacterial activity, Photocatalyst, Rhodamine dye

### Abstract

The present study reports an eco-friendly synthesis of chitosan/Fruit peel (CS NCs) nanocomposite using Citron by a biological method. The synthesized CS nanocomposite was characterized by using UV-visible spectroscopy; X-ray diffraction (XRD), scanning electron microscopy (SEM), and Fourier transform infrared spectroscopy (FTIR) techniques. The XRD analysis revealed tetragonal crystalline structure of CS nanocomposite. Electron microscopy images showed agglomeration of CS nanocomposite having agglomerate spherical shaped structure with an average size of 21–47nm. The observed bands around 400–500cm<sup>-1</sup> in the IR spectrum indicated the presence of Carboxylic and aromatic compounds, whereas bands at 1512 and 1745cm<sup>-1</sup> indicated the presence of amine groups (–NH<sub>2</sub>) which confirms the presence of CS in the CS/fruit peel nanocomposite. The synthesized nanocomposite showed potential antibacterial activity against various pathogens. Furthermore, CS nanocomposite acted as photocatalyst for the degradation of Rhodamine under UV light irradiation. In conclusion, as-synthesized CS nanocomposite can be used as bactericidal agent in textile industries and also as photocatalyst for dye degradation.

\*Corresponding Author: G. Annadurai ✉ [gannadurai@msuniv.ac.in](mailto:gannadurai@msuniv.ac.in)

## Introduction

Due to population growth, advances in the development of cities, the buildup of agricultural fruit and vegetable wastes and industrial wastes like organic dyes, pesticides, inorganic contaminants and detergents, and heavy and toxic metal ions, as well as the decomposition of toxic and poisonous gases and chemical species produced by various chemical industries, the natural ecosystem has been exposed to various natural and artificial hazardous problems (Ayala-Zavala *et al.*, 2011; Akbari *et al.*, 2011; Boukroufa *et al.*, 2015). Among them, the environmental release of different kinds and natures of dye effluents from diverse chemical industries and sources, such as dye stuffs, textiles, paint and varnishes, inks, plastics, pulp and paper, food, rubber, and cosmetics, is a significant cause of concern today throughout the world (Guntur *et al.*, 2018). Accordingly, it has been claimed that creating and constructing an effective and convenient removal protocol for these diverse sorts of pollutants from wastewater is becoming a pressing and challenging issue on a global scale. Many different industries use nanoparticles and nanocomposites in a variety of applications. Chitosan has a wide range of biological functions, including antibacterial and anti-inflammatory ones, and its role as a therapeutic polymer. A faster rate of wound healing is one of chitosan's many benefits, in addition to its biocompatibility, biodegradability, non-toxicity, and antibacterial activity (Liu *et al.*, 2006).

Chitosan is a linear polysaccharide made up of randomly distributed  $\beta$ -(1-4)-linked d-glucosamine and N-acetyl-d-glucosamine formed when chitin is deacetylated. Due to its biocompatibility, hemocompatibility, low toxicity, and biodegradation products, it has numerous medical applications (Asgari *et al.*, 2020). Chitosan films have been evaluated as tissue engineering scaffolds and as curative wound dressings. Additionally, it serves as a food preservative and coating for industrial food applications, extending shelf life (Ashassi-Sorkhabi and Kazempour, 2020). Citrus represents a wide range of significant fruit varieties that, because of

their distinctive nutritional makeup and high water content, are exposed to microbial contamination by phytopathogens during planting, harvesting, and commercialization (Wang *et al.*, 2022). Citrus nature is typically acidic (pH~2.2–4.0), which derive fungi to be the main responsible for most infections /deteriorations of these fruits (Cheng *et al.*, 2020; Salem *et al.*, 2022).

The investigation of the photocatalytic activity of chemically synthesized and to some extent environmentally obtained Chitosan nanocomposite for the degradation of various organic pollutants for the remediation of polluted water caused by various sources has previously been the focus of several studies and reports. Furthermore, earlier studies demonstrate that chitosan-based nanocomposites were made using a variety of chemical synthesis techniques for the recovery and treatment of wastewater contaminated by a variety of sources (Wu *et al.*, 2009; Bharathi *et al.*, 2010; Pashaei-Fakhri *et al.*, 2021). However, based on our knowledge as researchers, there is currently no published research on the environmentally friendly synthesis of chitosan nanocomposites in the presence of citrus peel extract and the reducing agent *Musa acuminata* as a cost-effective capping and reducing agent for the effective photocatalytic degradation of the dye methylene blue (Olana *et al.*, 2022; Azadmanesh *et al.*, 2021).

In this research, we employed citrus lemon juice to synthesize chitosan-based fruit peel nanocomposites (CS nanocomposite). UV-vis spectrophotometer, scanning electron microscope, X-ray diffraction assay, Fourier transform infrared spectroscopy, Particle Size Analyser and fluorescence spectroscopy were used to characterize the nanocomposites. Finally, photodegradation, antioxidant and antibacterial activity against fungal infections is performed to the nanocomposites which have been synthesized.

## Materials and methods

### Chemicals, Reagents, and Media

Analytical grade Raw Chitosan, Glacial Acetic Acid, Acrylic Acid, Methylmethacrylate, Ceric Ammonium

Nitrate and Rhodamine Dye was purchased from Sigma Aldrich Pvt Ltd, India. Bacterial isolates, Gram-positive *Staphylococcus aureus* and *Bacillus subtilis*, and Gram-negative *Escherichia coli*, *Enterobacter* and *Pseudomonas fluorescens* were procured from standard vendors.

#### Preparation of Citron Fruit Peel Powder

Citron fruit peel was obtained from a local area in Alwarkurichi. For powder processing, 20g of Fruit Peels were washed thoroughly with distilled water to remove the dirt particles adhere to it and cut into small pieces. The pieces of peels were allowed to shade dry at the temperature 25-30 °C for a period of 96 hours. The dried fruit peels were made into coarse powder using mixer and blender with the help of a sieve. The fine powder was collected and stored in an air tight container for further use.

#### Synthesis of Chitosan Nanocomposite using Citron Fruit Peel Powder

Chitosan Nanocomposite has been synthesized as follows. 1g of the raw Chitosan powder was dissolved in 95ml of distilled water. To this mixture, 5mL of Acetic acid was added. The stirred reaction was carried out for 20 min. Then, 1 g of citron fruit peel powder was added under stirring for 30 mins. The reaction was carried out under nitrogen atmosphere with a flow rate of 1ml/min in a boiling water bath. After the completion of reaction, the obtained final product is dried in hot air oven at 60<sup>0</sup> C for 2 h.

#### Photocatalytic Activity

The photocatalytic activity of Chitosan nanocomposite was evaluated on the degradation of Rhodamine (Merck, India) in an aqueous solution under UV light (300 W/m<sup>2</sup>, Osram) illumination. A known weight of the catalyst, 0.1g was added to a known volume of 0.2 L dye that resulted in a suspension. The suspension was stirred for uniform exposure of the catalyst to light. The distance between the lamp and the base of the beaker under UV illumination was 13cm. Each experiment was conducted every 180 min with a 10ml sample of a liquid drawn every 20 min. The degradation of the

dye was monitored after the removal of photocatalyst by centrifugation at 3000 rpm for 20 min. The decreased absorbance was measured at regular intervals of time from 0 to 180 min by using the Shimadzu UV1650 PC spectrometer.

#### Antibacterial Property

The antibacterial property of the Chitosan nanocomposite was determined by using the bacterial species including the pathogenic bacteria such as Gram-positive *Staphylococcus aureus* and *Bacillus subtilis*, and Gram-negative *Escherichia coli*, *Enterobacter*, and *Pseudomonas fluorescens* by the well diffusion method. The different concentrations used were at 25µl, 50µl, 75µl and 100µl for the identification of antimicrobial activity of the above bacterial species. All the plates were incubated at 37°C for 24 hours, and the zone of inhibition of bacteria was measured.

#### Result and discussion

##### Ultraviolet (UV) and Florescence (fl) spectroscopy

The UV-vis spectra were measured to characterize optical properties of Chitosan Nanocomposite (Figure 1(a)). The absorption spectrum was shows a characteristic surface plasmon resonance (SPR) band of Chitosan Nanocomposite between 200 and 600nm, with a peak around 380nm. The biomolecule of fruit peel coated Chitosan Nanocomposite are well disseminated in liquids and relatively stable for up to three months, as seen by the white colour of the colloidal solution (Al-Radadi, 2019).

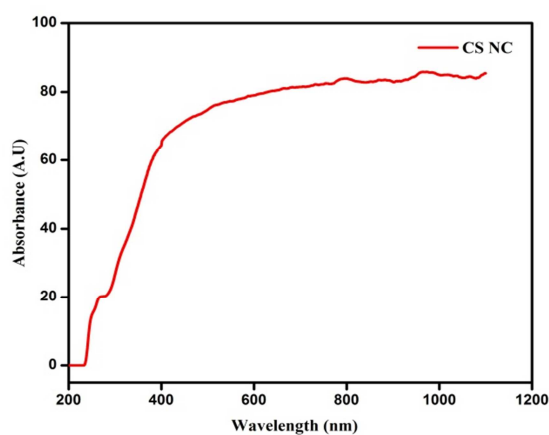


**Fig. 1(a).** Optical spectrum of Chitosan Nanocomposite.

As shown in Fig.1b, the fluorescence spectra of Chitosan Nanocomposite were recorded at room temperature using a fluorescence spectrophotometer. Measurements were taken in the 350-900nm wavelength range. As shown in Fig.1 (b), maximum wavelength emission intensities were gathered from the experiments, and emission values were shown as wavelength (nm) versus intensity (A.U). Chitosan Nanocomposite has three distinct peaks, as seen in Fig. 1b. The lower emission peak was recorded at 351 and 435nm and was attributed to the Chitosan Nanocomposite production, whereas the higher emission peak was observed at 574nm and was related to the surface defects (Rehan *et al.*, 2018). For assessing energy levels, fluorescence spectra were the preferred method. The fluorescence intensity increased as the size of Chitosan Nanocomposite increased.

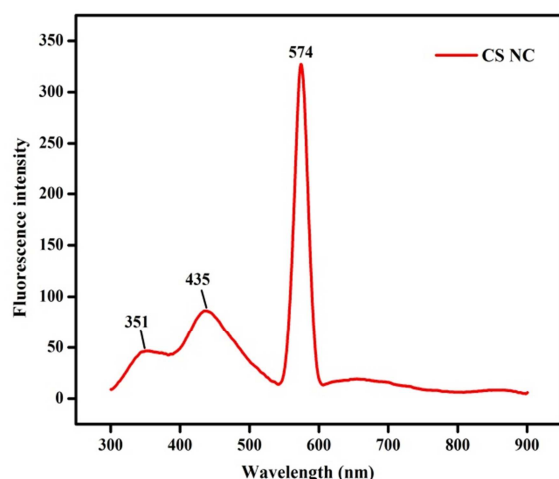


**Fig.1 (b).** Fluorescence spectrum of Chitosan Nanocomposite.

*X-ray diffraction (XRD)*

Figure 2 shows the X-ray diffraction pattern of Chitosan Nanocomposite synthesized using fruit peel. Diffraction peaks were at 2θ values of 20° and 42° corresponding to (111) and (200) crystallographic planes, respectively. These diffraction peaks are characteristic of a face centered cubic structure of Chitosan Nanocomposite (JCPDS Card No. 04-0783) (Unuofin *et al.*, 2020). There are a few other peaks present due to crystalline impurities in the sample. These results show that the fruit peel reduced chitosan ions into Chitosan Nanocomposite. The

crystal size of the nanocomposites was further determined and verified by X-ray diffraction using Scherer’s formula (Shah *et al.*, 2018). The calculated crystalline size was approximately 20nm, similar to the results obtained by scanning electron microscopy.

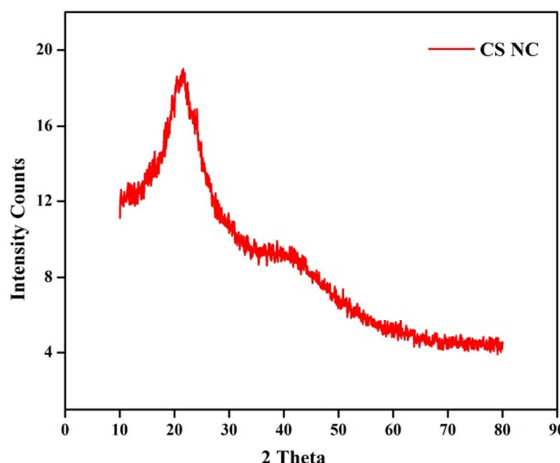


**Fig. 2.** XRD spectrum of Chitosan Nanocomposite.

*Dynamic light scattering (DLS)*

The Chitosan Nanocomposite were ultrasonically processed and suspended in an ethanol solution. A particle size analyzer was used to estimate the sizes of the agglomerated colloids in the suspensions (PSA).

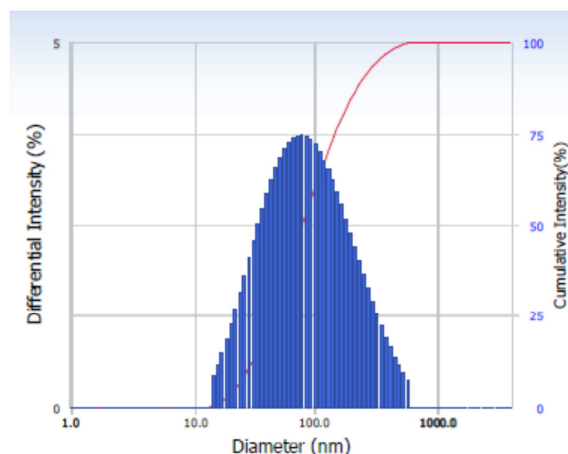


**Fig. 3.** DLS image of Chitosan Nanocomposite.

The particle size was determined to be 75nm, which is in good agreement with the crystallite size of, which is twice that of the crystallite size (Akbari *et al.*, 2011). Figure 3 depicts the particle size distribution and average particle size of Chitosan Nanocomposite. A coherent source of light is directed at a particle

suspension in DLS, where it is scattered (Guntur *et al.*, 2018). Because of the continually fluctuating distances between the scatterers, the scattering fluctuates with time due to the random Brownian motion of the particles. When are evaluated, the size of ionic liquid and fruit peel mediated nanocomposites as assessed by DLS may appear smaller than plant mediated nanocomposites without ionic liquid. Fruit-mediated nanocomposites aggregate quickly in most investigations. After four hours of ageing, DLS is documented in this study. The size distribution profile of nanocomposites in suspension has previously been determined using DLS.

*Fourier transforms infrared (FTIR) spectroscopy*

FTIR analysis carried out to characterize the Chitosan Nanocomposite obtained from plant is shown in Figure 4. FTIR analysis has been done in the wave number range from 450/cm to 4000/cm. In solutions, prominent bands of absorbance were observed at around 3431, 2923, 1734, 1641, 1384, 1159, 639 and 537cm<sup>-1</sup>. The observed peaks denote N–H stretch1°, 2° amines, amides, C–H stretch alkanes, Nitrile C=N Stretch, C=O (saturated aldehyde) Aldehydes & Ketones, C=C stretch (conjugated) alkenes, C-F stretch alkyl halides, C-N Amines, C-H bend (mono) aromatic compound, C–Br stretch alkyl halides respectively as shown Table 1.

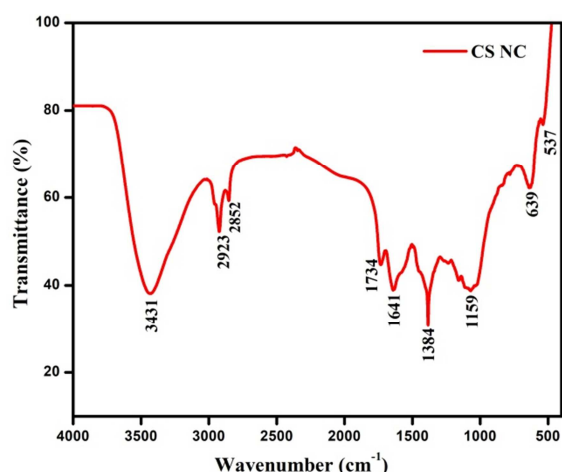


**Fig. 4.** FTIR spectrum of Chitosan Nanocomposite.

These bands denote stretching vibrational bands responsible for compounds like flavonoids and terpenoids (Kanakarajan *et al.*, 2018) and so may be

held responsible for efficient capping and stabilization of obtained Chitosan Nanocomposite. The peaks indicated the existence of many functional groups in the fruit peel using Chitosan Nanocomposite liable for the formation of stable (Olajire *et al.*, 2017; Satapathy *et al.*, 2015).

**Table 1.** Peak table of Chitosan Nanocomposite.

| SL | Peak (cm <sup>-1</sup> ) | Functional Group                             |
|----|--------------------------|--|
| 1  | 3431                     | N–H stretch1°, 2° amines, amides             |
| 2  | 2923                     | C–H stretch alkanes                          |
| 3  | 1734                     | C=O (saturated aldehyde) Aldehydes & Ketones |
| 4  | 1641                     | C=C stretch (conjugated) alkenes             |
| 5  | 1384                     | C-F stretch alkyl halides                    |
| 6  | 1159                     | C-N Amines                                   |
| 7  | 639                      | C-H bend (mono) aromatic compound            |
| 8  | 537                      | C–Br stretch alkyl halides                   |

*Scanning electron microscopy (SEM)*

The SEM images of the Chitosan Nanocomposite are shown in Figure 5. The SEM images justify the structural and morphological behavior of the Chitosan Nanocomposite. It is seen that Chitosan Nanocomposite of different shapes were obtained in case of citron fruit peel being used as reducing and capping agents. Fruit peel using Chitosan formed approximately cube, rod and trapezium nanostructures Chitosan Nanocomposite, respectively (Banerjee *et al.*, 2014). This may be due to availability of different quantity and nature of capping agents present in the different fruit peel. This is also supported by the shifts and difference in areas of the peaks obtained in the FTIR analysis.

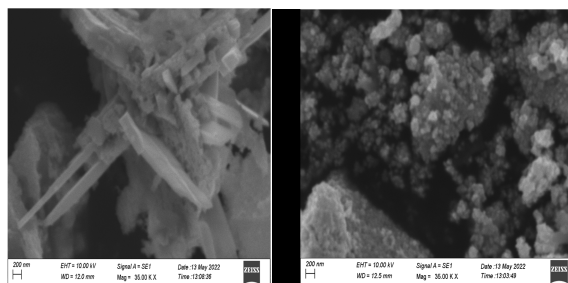


**Fig. 5.** SEM image of Chitosan Nanocomposite.

*Photocatalytic properties of Chitosan Nanocomposite*

The degradation of the Rhodamine dye under UV irradiation was used to assess the photocatalytic

activity of Chitosan nanocomposite. Rhodamine dye is a common industrial contaminant and an important class of synthetic organic dyes used in the textile industry (Badr *et al.*, 2008). The efficiency of degradation was improved due to the interaction between the photocatalyst and the dye molecule. Under UV irradiation, the produced silver nanoparticles decolorized Rhodamine dye by 92% in about 180 minutes, suggesting full breakdown of dye molecules by chitosan nanocomposite. The progressive disappearance of Rhodamine dye's absorption bands revealed that the functional groups responsible for the dye's distinctive hue were being broken down (Ferdosi *et al.*, 2019). Figure 7 shows the time-dependent UV-vis absorption spectra of Rhodamine dye in the presence of chitosan nanocomposite.

*Mechanism of Photocatalytic Catalytic Degradation of the Dye*

Fig. 6. depicts the degradation of Rhodamine dye as a light-dependent process. The dye is first adsorbed on the surface of the catalyst (in this example, Chitosan nanocomposite), then exposed to ultraviolet light to excite valence electrons and allow them to move from the valence band to the conduction band; a positive hole  $h^+$  is lifted inside the valence band during this process. (Yasmin *et al.*, 2020).

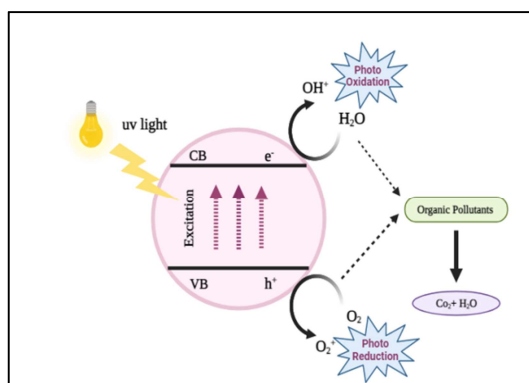


**Fig. 6.** Reaction Mechanism for the Degradation of Rhodamine.

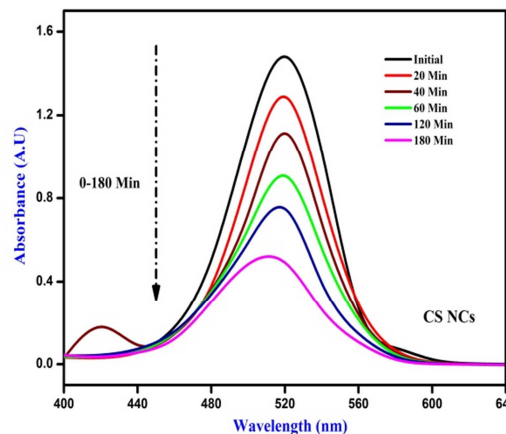
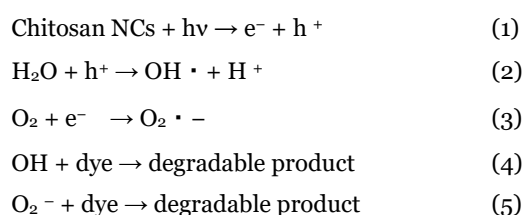


**Fig. 7.** UV-visible spectra of Rhodamine dye degradation with Chitosan Nanocomposite.

Positive holes and free electrons react with adsorbed water molecules on the photocatalyst's surface, yielding  $\cdot\text{OH}$  radicals, while free electrons convert dissolved oxygen to superoxide anion  $\text{O}_2 \cdot^-$  radicals. These light-generated radicals breakdown the dye molecules into simple molecules like  $\text{CO}_2$  and  $\text{H}_2\text{O}$  (Ferdosi *et al.*, 2019; Taha *et al.*, 2020).

*Antibacterial activity*

The antimicrobial activity of chitosan nanocomposite was tested against laboratory test organisms of biological importance, i.e., *Staphylococcus aureus*, *Bacillus subtilis*, *Enterobacter*, and *Pseudomonas fluorescens*. Figure 8 shows the photographs taken after antimicrobial measurements for sample prepared by a 24-h reaction time (Suriyakala *et al.*, 2022). *Pseudomonas fluorescens* had a clear zone of inhibition for all the study concentrations with the highest of 3.5mm for 100 $\mu\text{l}$  (Table 2). *Escherichia coli*, *Staphylococcus aureus*, *Bacillus subtilis*, and *Enterobacter* had 2.4, 3.2, 2.8 and 2.6mm for 100 $\mu\text{g}$ . The antimicrobial activity of silver nanoparticles depends on their shape and size (Liu *et al.*, 2006). These results showed that the nanoparticles exhibited good activity against gram positive *Staphylococcus aureus* and *Bacillus subtilis*, gram negative *Enterobacter* and *Pseudomonas*. Thus, the nanoparticles may be considered to be a good antibiotic material. These studies on the antibacterial effect could be appropriately used in industrial applications, therapeutic formulations and environmental remediation studies (Qi *et al.*, 2004).

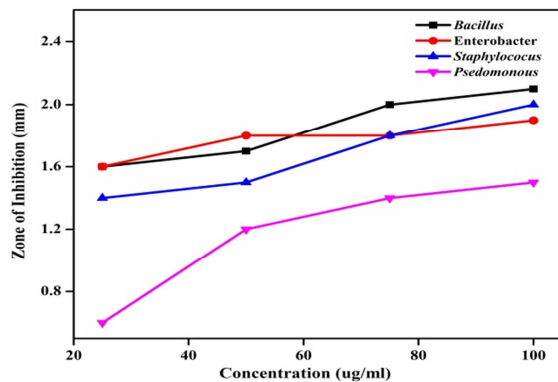


**Fig. 8.** Zone of inhibition of CS NCs various bacterial strains.

**Table 2.** Zone of inhibition of CS NCs against selected bacterial Strains.

| Concentration | Zone of Inhibition (mm in diameter) |                   |                              |                         |
|---------------|-------------------------------------|-------------------|------------------------------|-------------------------|
|               | <i>Bacillus</i> sp.                 | Entero bacter sp. | <i>Staphylococcus aureus</i> | <i>Pseudo monas</i> sp. |
| 25µl          | 1.6                                 | 1.6               | 1.4                          | 0.6                     |
| 50µl          | 1.7                                 | 1.8               | 1.5                          | 1.2                     |
| 75µl          | 2.0                                 | 1.8               | 1.8                          | 1.4                     |
| 100µl         | 2.1                                 | 1.9               | 2.0                          | 1.5                     |

**Conclusion**

The CS NCs was successfully synthesized using citron fruit peel, and the properties were investigated. The crystalline structure of the produced CS NCs was confirmed by XRD examination. FTIR spectra of chitosan composites exhibit the presence of characteristic organic and inorganic absorption bands. SEM was used to assess morphologies and vibrational modes, DLS was used to determine surface charge and stability, and TGA was used to determine stability. The synthesized CS NCs were also effective in the degradation of Rhodamine dye. Antibacterial activity of the prepared samples was confirmed by the well diffusion method against grampositive *Bacillus subtilis* and *Staphylococcus aureus* and gram-negative *Enterobacter* and *Pseudomonas fluorescens* bacteria strains. The characterization results evidently demonstrated the formation of CS NCs. The antibacterial results confirmed that all the samples exhibited antibacterial activities against the bacteria strains. Considering the results, the CS NCs can be used as an operative antibacterial agent against hazardous bacterial pathogens.

**Acknowledgements**

In order to complete this study S. Amutha (Reg.No.21124012032015) appreciates the Sri Paramakalyani Centre for Excellence in Environmental Science at Manonmaniam Sundaranar University in Alwarkurichi, India

**References**

**Akbari B, Tavandashti MP, Zandrahimi M.** 2011. Particle size characterization of nanoparticles—a practical approach. *Iranian Journal of Materials Science and Engineering* **2**, 48-56.

**Al-Radadi NS.** 2019. Green synthesis of platinum nanoparticles using Saudi’s Dates extract and their usage on the cancer cell treatment. *Arabian Journal of Chemistry* **12**, 330-349.

**Asgari E, Sheikhmohammadi A, Yeganeh J.** 2020. Application of the Fe<sub>3</sub>O<sub>4</sub>·chitosan nano-adsorbent for the adsorption of metronidazole from wastewater: Optimization, kinetic, thermodynamic and equilibrium studies. *International Journal of Biological Macromolecules* **164**, 694-706.

**Ashassi-Sorkhabi H, Kazempour A.** 2020. Chitosan, its derivatives and composites with superior potentials for the corrosion protection of steel alloys: A comprehensive review. *Carbohydrate Polymers* **237**, 116110.

**Ayala-Zavala JF, Vega-Vega V, Rosas-Domínguez C, Palafox-Carlos H, Villa-Rodríguez J A, Siddiqui W.** 2011. Agro-industrial potential of exotic fruit byproducts as a source of food additives. *Food Res. Int.* **44**, 1866–1874.

**Azadmanesh F, Pourmadadi M, Zavar Reza J, Yazdian F, Omidi M, Haghirosadat BF.** 2021. Synthesis of a novel nanocomposite containing chitosan as a three-dimensional printed wound dressing technique: Emphasis on gene expression. *Biotechnology Progress* **e3132**, 1-13.

**Badr Y, Abd El-Wahed MG, Mahmoud MA.** 2008. Photocatalytic degradation of methyl red dye by silica nanoparticles. *Journal of Hazardous Materials* **154**, 245-253.

- Banerjee P, Satapathy M, Mukhopahayay A, Das P.** 2014. Leaf extract mediated green synthesis of silver nanoparticles from widely available Indian plants: synthesis, characterization, antimicrobial property and toxicity analysis. *Bioresources and Bioprocessing* **1**, 1-10.
- Bharathi S, Nataraj D, Mangalaraj D, Masuda Y, Senthil K, Yong K.** 2010. Highly mesoporous  $\alpha$ -Fe<sub>2</sub>O<sub>3</sub> nanostructures: preparation, characterization and improved photocatalytic performance towards Rhodamine B (rhb). *J. Phys. D. Appl. Phys* **43**, 015501.
- Boukroufa M, Boutekedjiret C, Petigny L, Rakotomanomana N, Chemat F.** 2015. Bio-refinery of orange peels waste: a new concept based on integrated green and solvent free extraction processes using ultrasound and microwave techniques to obtain essential oil, polyphenols and pectin. *Ultrason. Sonochem* **24**, 72-79.
- Cheng Y, Lin Y, Cao H, Li Z.** 2020. Citrus postharvest green mold: recent advances in fungal pathogenicity and fruit resistance. *Microorganisms* **8**, 449.
- Ferdosi E, Bahiraei H, Ghanbari D.** 2019. Investigation of the photocatalytic activity of CoFe<sub>2</sub>O<sub>4</sub>/ZnO and CoFe<sub>2</sub>O<sub>4</sub>/ZnO/Ag nanocomposites for purification of dye pollutants. *Separation and purification technology* **211**, 35-39.
- Guntur SR, Kumar NS, Hegde MM, Dirisala VR.** 2018. In vitro studies of the antimicrobial and free-radical scavenging potentials of silver nanoparticles biosynthesized from the extract of *Desmostachya bipinnata*. *Analytical chemistry insights* **13**, 117.
- Kanakarajan S, Selvaraj R, Kamalanathan.** 2018. *Achyranthes aspera* mediated green synthesis of silver nanoparticles. *Indo American Journal of Pharmaceutical Sciences* **5**, 64-73.
- Liu N, Chen XG, Park HJ, Liu CG, Liu CS, Meng XH, Yu LJ.** 2006. Effect of MW and concentration of chitosan on antibacterial activity of *Escherichia coli*. *Carbohydrate polymers* **64**, 60-65.
- Olajire AA, Kareem A, Olaleke A.** 2017. Green synthesis of bimetallic Pt@ Cu nanostructures for catalytic oxidative desulfurization of model oil. *Journal of Nanostructure in Chemistry* **7**, 159-170.
- Olana MH, Sabir FK, Bekele ET, Gonfa BA.** 2022. *Citrus sinensis* and *Musa acuminata* peel waste extract mediated synthesis of TiO<sub>2</sub>/rGO nanocomposites for photocatalytic degradation of methylene blue under visible light irradiation. *Bioinorganic Chemistry and Applications* **2**, 25-31.
- Pashaei-Fakhri S, Peighambaroust SJ, Foroutan R, Arsalani N, Ramavandi B.** 2021. Crystal violet dye sorption over acrylamide/graphene oxide bonded sodium alginate nanocomposite hydrogel. *Chemosphere* **270**, 129419.
- Qi L, Xu Z, Jiang X, Hu C, Zou X.** 2004. Preparation and antibacterial activity of chitosan nanoparticles. *Carbohydrate research* **339**, 2693-2700.
- Rehan M, El-Naggar ME, Mashaly HM, Wilken R.** 2018. Nanocomposites based on chitosan /silver/clay for durable multi-functional properties of cotton fabrics. *Carbohydrate polymers* **182**, 29-41.
- Salem MF, Abd-Elraoof WA, Tayel AA, Alzuaibr FM, Abonama OM.** 2022. Antifungal application of biosynthesized selenium nanoparticles with pomegranate peels and nanochitosan as edible coatings for citrus green mold protection. *Journal of Nanobiotechnology* **20**, 182.
- Satapathy MK, Banerjee P, Das P.** 2015. Plant-mediated synthesis of silver-nanocomposite as novel effective azo dye adsorbent. *Applied Nanoscience* **5**, 1-9.
- Shah A, Hussain I, Murtaza G.** 2018. Chemical synthesis and characterization of chitosan/silver nanocomposites films and their potential antibacterial activity. *International journal of biological macromolecules* **116**, 520-529.
- Suriyakala G, Sathiyaraj S, Devanesan S, AlSalhi MS, Rajasekar A, Maruthamuthu MK, Babujanathanam R.** 2022. Phytosynthesis of silver nanoparticles from *Jatropha integerrima* Jacq. flower extract and their possible applications as antibacterial and antioxidant agent. *Saudi Journal of Biological Sciences* **29**, 680-688.

**Taha A, Ben Aissa M, Dana E.** 2020. Green synthesis of an activated carbon-supported Ag and ZnO nanocomposite for photocatalytic degradation and its antibacterial activities. *Molecules* **257**, 1586.

**Unuofin JO, Oladipo AO, Msagati TAM, Lebelo SL, Meddows-Taylor S, More GK.** 2020. Novel silver-platinum bimetallic nanoalloy synthesized from *Vernonia mespilifolia* extract: Antioxidant, antimicrobial, and cytotoxic activities. *Arabian Journal of Chemistry* **13**, 6639-6648.

**Wang Z, Sui Y, Li J, Tian X, Wang Q.** 2022. Biological control of postharvest fungal decays in citrus: a review. *Critical Reviews in Food Science and Nutrition* **62**, 861-870.

**Wu S, Cao H, Yin S, Liu X, Zhang X.** 2009. Amino acid-assisted hydrothermal synthesis and photocatalysis of SnO<sub>2</sub> nanocrystals. *J. Phys. Chem. C* **113**, 17893-17898.

**Yasmin S, Nouren S, Bhatti HN, Iqbal DN, Iftikhar S, Majeed J, Mustafa R, Nisar N, Nisar J, Nazir A, Iqbal M.** 2020. Green synthesis, characterization and photocatalytic applications of silver nanoparticles using *Diospyros lotus*. *Green Processing and Synthesis* **9(1)**, 87-96.